GSA Data Repository 2017098; doi:10.1130/G38600.1

Dating Icelandic glacial floods using a new viscous remanent magnetization method – Supplementary Material

Thomas Berndt and Adrian R. Muxworthy

January 24, 2017

DR1 Fieldwork

Fig. DR1 shows photos of some of the boulders sampled in Iceland.

(a) Boulder with the Sólheimajökull in the background.

(b) Boulder S2 at the Sólheimajökull flood basin.

(c) Boulder S14 at the Sólheimajökull.

(d) Drilling a boulder at the Kotarjökull flood basin.

(e) Boulder K3 at the Kotarjökull flood basin.

(f) Boulder K4 at the Kotarjökull.

(g) Drilling boulder K9 at the Kotarjökull flood basin.

(h) Boulder M1 at the Markarfljot.

Figure DR1: Typical boulders sampled in Iceland.

DR2 Applicability of VRM theories of Néel (1949) and Walton (1980)

In the literature on viscous remanent magnetization dating (e.g. Kent, 1985; Kent and Miller, 1987; Smith and Verosub, 1994; Sato et al., 2014; Muxworthy et al., 2015), there is a general disagreement on which one of two theoretical framework to use: (1) the expression derived by Pullaiah et al. (1975) based on Néel (1949) theory of single-domain (SD) grains

$$\frac{T_A}{M_s\left(T_A\right)H_K\left(T_A\right)}\ln\left(\frac{t_A}{\tau_0}\right)=\frac{T_D}{M_s\left(T_D\right)H_K\left(T_D\right)}\ln\left(\frac{t_D}{\tau_0}\right)\,, \tag{DR1}$$

where T_A and t_A are the VRM acquisition temperature and time, respectively (i.e. temperature and time in the field), and T_D and t_D are demagnetization temperature and time in the laboratory experiment, respectively, or (2) the expression by Middleton and Schmidt (1982) based on Walton (1980) theory of grain-size distributions of SD grains,

$$\frac{T_A}{M_s\left(T_A\right)H_K\left(T_A\right)}\left[\ln\left(\frac{t_A}{\tau_0}\right)\right]^r=\frac{T_D}{M_s\left(T_D\right)H_K\left(T_D\right)}\left[\ln\left(\frac{t_D}{\tau_0}\right)\right]^r\,, \tag{DR2}$$

where r depends on the grain-size distribution and equals approximately 2 for a log-normal distribution. The two equation, although similar in form, do, however, describe very different physical situations, and from a theoretical perspective. Enkin and Dunlop (1988) point out that eq. DR2 relates time and temperature for a constant value of the total magnetic moment M, while equation (DR1) relates time and temperature for a constant grain size, which is why the grain size distribution matters in Walton's equation, but not in Néel's equation. Here, we summarize the argument of Enkin and Dunlop (1988) to show that eq. (DR1) is appropriate for VRM dating.

DR2.1 Demagnetizing all magnetized grains: Néel (1949) / Pullaiah et al. (1975)

Pullaiah et al. (1975) rearranged the relaxation time equation

$$\frac{1}{\tau}=\frac{1}{\tau_0}\exp\left\{-\frac{\mu_0 V M_s H_K}{kT}\right\}\,, \tag{DR3}$$

from Néel (1949) theory of magnetic single-domain (SD) grains to obtain eq. (DR1), where τ_0 is the atomic attempt time, μ_0 is the vacuum permeability, V is the grain volume, M_s is the spontaneous magnetization, H_K is the microscopic coercivity, and k is the Boltzmann constant. Eq. (1) used in this study follows immediately from eq. (DR1) by assuming shape anisotropy, for which (Dunlop and Özdemir, 1997)

$$H_K\left(T\right)=\Delta N M_s\left(T\right)\,, \tag{DR4}$$

where ΔN is the shape anisotropy factor, and the analytical approximation for the spontaneous magnetization of (titano)magnetite (Dunlop and Özdemir, 1997)

$$M_s\left(T\right)=M_s\left(0°\mathrm{C}\right)\sqrt{1-\frac{T}{T_C}}\,. \tag{DR5}$$

The physical meaning of eq. (DR3) is to relate the relaxation time t to the blocking temperature T for any particular grain of a given volume, shape, coercivity, etc. All grains larger than the blocking volume V_B or with a higher microscopic coercivity H_K in the equation will be blocked, while all smaller or lower-coercivity grains will be unblocked and align to the ambient field. This is illustrated in Fig. DR2, where grains above the contour lines are blocked at the indicated temperature and grains below the contour lines are unblocked.

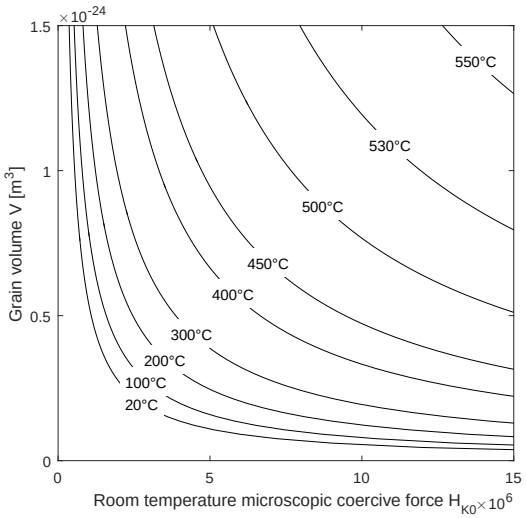

Figure DR2: Schematic illustration of the blocking condition (Néel, 1949) eq. (DR3) for $\tau = 100\,\mathrm{s}$. Grains below the contour lines are superparamagnetic at the given temperatures, and those above are blocked.

DR2.2 Producing VRMs with a given magnetic moment: Walton (1980) / Middleton and Schmidt (1982)

Walton (1980) derived a theory based on Néel (1949) theory to describe the total magnetic moment of assemblies of SD grains of different sizes produced over a time t_A at a temperature T_A in the field. He integrated eq. (DR3) over both volume V and coercivity H_K to calculate the total magnetic moment of such an assembly. Crucially, the average magnetic moment $\bar{m}$ of a grain of a given volume and coercivity is given by a Maxwell-Boltzmann distribution (Néel, 1949)

$$\bar{m} = \tanh\left\{\frac{\mu_0 V M_s H_0}{kT}\right\}, \tag{DR6}$$

where H_0 is the ambient magnetic field. This means that, grains larger than the blocking volume V_B can produce different magnetic moments, depending on the temperature at which they became blocked and the ambient field. Moreover, the magnetic moment is proportional to the grain's volume; for an assembly of a given number of grains, for grain size distributions with relatively more small grains, the magnetic moment will be weaker than for one with relatively more large grains.

Eq. (DR2) was derived by Walton (1980) by approximating a lognormal grain-size distribution; the power r in the equation arises from this. This equation relates magnetic moments acquired by a sample at two different temperatures, T_A and T_D: the equation predicts for what time t_A and t_D these two moments are equal. Applying this equation to VRM dating is incorrect: it would correspond to producing a magnetic moment in the laboratory that is equal to the moment of the VRM that the sample acquired in the field (note that t_D and T_D do not refer to demagnetization in this case). In Fig. DR2 this corresponds to magnetizing two different sets of grains: the naturally acquired magnetic moment is carried by the grains below the contour line of T_A, say, 200°C, while the lab-acquired magnetic moment is carried by the grains below the contour line of T_D, say, 300°C; eq. (DR2) affirms that the total magnetic moments of all grains below these two respective lines are equal. This also means that for different grain-size distributions, t_D and T_D will differ to produce the same paleointensity. As pointed out by Enkin and Dunlop (1988), the equations by Walton (1980) would correspond to replacing the naturally acquired VRM by a laboratory VRM of equal intensity

at a higher temperature, since part of the natural VRM is already erased in the short-term heating to the higher temperature.

It is noteworthy that eq. (DR2) only applies to magnetic acquisition and does not apply demagnetization experiments: for demagnetization, the Maxwell-Boltzmann distribution eq. (DR6) equals zero (as the field H_0 is zero). As the theory predicts what time and temperature produces a given total magnetic moment, in the demagnetization case, eq. (DR2) refers to the time t_D and temperature T_D to *remove* the same magnetic moment as is removed over time t_A and temperature T_A. The only way to remove the same magnetic moment is to demagnetize the same grains, which are given by eq. (DR1) (Néel, 1949; Pullaiah et al., 1975), as used by the most recent VRM dating studies (Sato et al., 2014; Muxworthy et al., 2015). This has to be independent of the grain size distribution, as any grain size distribution will have zero moment once it has approached its equilibrium state for zero field; the power r in eq. (DR2) arising from the grain-size distribution disappears in the demagnetization case, reducing it to eq. (DR1).

DR2.3 Conclusion

While previous works have often taken a rather phenomenological approach, trying both eqs. (DR1) and (DR2) and observing which one matches experiments best, it is important to understand the different situations the two equations describe: Eq. (DR1) by Pullaiah et al. (1975) describes which grains are blocked and unblocked at a given temperature and time, whereas eq. (DR2) by Walton (1980) describes the magnetic moments that are produced at a given temperature and time. Furthermore eq. (DR1) applies for both magnetization and demagnetization, eq. (DR2) only to acquisition. Therefore only eq. (DR1) by Néel (1949) / Pullaiah et al. (1975) is appropriate for VRM dating.

DR3 Choice of demagnetization temperatures in curved demagnetization plots

Even for pure single-domain (SD) magnetite samples, demagnetization plots often appear curved, because of the statistical nature of remanence acquisition of SD grains (Néel, 1949): grains do not block/unblock instantaneously but their probability of flipping their magnetic moment vector to align with an external field increases with temperature, with a sharp increase around a particular temperature that justifies the concept of a blocking temperature. As this increase is not instantaneous, however, a standard is needed to select one unique point to use as "the" demagnetization temperature of the VRM. Fig. DR3 shows a schematic drawing of a demagnetization plot with a horizontal original remanent magnetization and a vertical VRM, and a typical curvature. Four possible choices of demagnetization temperatures are indicated. Two obvious choices are the extreme points: the point were the curvature starts and the point were the curvature ends. A third intuitive choice is the middle point: the point were the direction is intermediate to the VRM and the ChRM. From a mathematical perspective, the vector magnetization of a sample is found by integrating over all present grain volumes,

$$\mathbf{M}_r = \int M_s V f\left(V\right) \mathbf{n}\left(V\right)\, dV\,, \tag{DR7}$$

where f is the grain volume distribution and $\mathbf{n}$ is the magnetic moment vector (normalized by the saturation magnetic moment) of the grains of volume V. The differential vector magnetization, that is the direction of the demagnetization plot at each point, is given by

$$\frac{d\mathbf{M}_r}{dT} = \frac{d\mathbf{M}_r}{dV}\frac{dV}{dT_B} = M_s V f\left(V\right)\mathbf{n}\left(V\right) + \frac{dM_s}{dT}\int V f\left(V\right)\mathbf{n}\left(V\right)\, dV\,, \tag{DR8}$$

where the second term arises when the remanence $\mathbf{M}_r$ is measured at elevated temperature, i.e. for continuous thermal demagnetization (CTD). For stepwise thermal demagnetization the second term vanishes,

$$\frac{d\mathbf{M}_r}{dT} = M_s V f\left(V\right)\mathbf{n}\left(V\right)\,. \tag{DR9}$$

To simplify the mathematics, we will continue using this expression, even though CTD is used. This is a reasonable approximation for the low temperatures that are of interest to studies of VRMs, as M_s does not vary much at low temperatures (for stoichiometric magnetite, M_s changes by less than 15% from room temperature to 150°C, by eq. DR5). The normalized magnetic moment $\mathbf{n}$ is the sum of the primary remanent magnetization (characteristic remanent magnetization, ChRM) component $\mathbf{n}_{ChRM}$, that decays exponentially with time t_A (the time of VRM acquisition, not the time of ChRM acquisition), and the VRM component that approaches exponentially the equilibrium state $\mathbf{n}_{VRM,eq}$,

$$\frac{d\mathbf{M}_r}{dT} = M_s V f\left[\mathbf{n}_{ChRM,eq}\exp\left\{-\frac{t_A}{\tau}\right\} + \mathbf{n}_{VRM,eq}\left(1-\exp\left\{-\frac{t_A}{\tau}\right\}\right)\right]\,, \tag{DR10}$$

where τ is the relaxation time. Assuming that the equilibrium states of the ChRM and the VRM only differ in the direction of the applied field, $\mathbf{v}_{ChRM}$ and $\mathbf{v}_{VRM}$, respectively, and not in intensity (which is not strictly true due to the different acquisition temperatures according to eq. (DR6), and due to possible changes in field intensity),

$$\frac{d\mathbf{M}_r}{dT} = M_s V f n_{eq}\left[\mathbf{v}_{ChRM}\exp\left\{-\frac{t_A}{\tau}\right\} + \mathbf{v}_{VRM}\left(1-\exp\left\{-\frac{t_A}{\tau}\right\}\right)\right]\,. \tag{DR11}$$

Hence the differential direction at any given blocking temperature exponentially approaches the VRM direction with acquisition time (Fig. DR4). The definition of the blocking temperature according to

Néel (1949) is that the acquisition time equals the relaxation time, i.e. $t_A = \tau$, in which case the differential direction is given by the vector sum of $e^{-1}\mathbf{v}_{ChRM} + \left(1 - e^{-1}\right)\mathbf{v}_{VRM}$, i.e., the magnetic moment of the VRM is $\left(1 - e^{-1}\right) \approx 0.63$ times its equilibrium value (Fig. DR3); this is point corresponds to the blocking temperature of the VRM according to the definition $t_A = \tau$ by Néel (1949). This temperature is significantly lower than the end point, where the VRM is completely demagnetized.

We can exclude the two extreme points of curvature for both the theoretical reason just outlined, and for the practical reason that they are difficult to determine without an arbitrary threshold of where the curvature is considered to start and end (Fig. DR4). Hence, from a theoretical perspective, the $\left(1 - e^{-1}\right)$ point best describes the blocking condition, while the end point, a choice made by Muxworthy et al. (2015) (labeled "0" in Fig. DR3), would be expected to over-estimate blocking temperatures and hence age estimates. In this work we use the point where the VRM is at 0.5 times its equilibrium value is chosen for the practical reason that it is easily determined and close to the theoretical $\left(1 - e^{-1}\right)$ point. This is probably more similar to the inflection points determined "by eye" by Sato et al. (2014) compared to the approach by Muxworthy et al. (2015).

For ideal non-interacting SD magnetite samples, the temperature range between the points "0" and "1" (Fig. DR3) would theoretically be around 10°C, which would roughly translate into an order-of-magnitude difference in VRM dating age estimates. In real samples, the curvature is often larger due to non-SD behavior, which would further increase the inaccuracy of the age estimate.

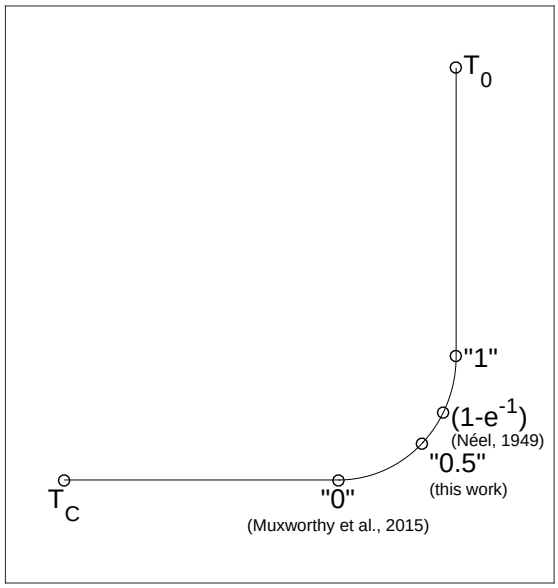

Figure DR3: Schematic drawing of a curved Zijderveld (1967) plot of a primary TRM vertical and a secondary horizontal VRM, where the curvature is due to the statistical nature of blocking of SD grains. Four possible choices of demagnetization temperatures of the VRM are indicated, with the numbers indicating the percentage of the equilibrium normalized magnetization $\mathbf{n}_{eq}$ of the VRM at each of the points.

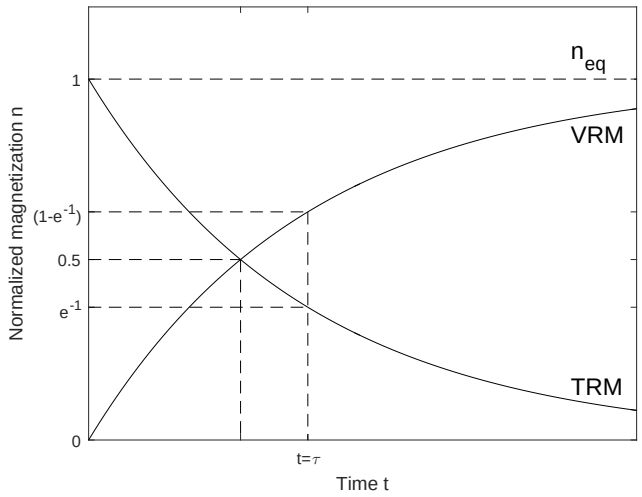

Figure DR4: Schematic drawing of secondary VRM acquisition and simultaneous decay of the primary TRM. Points where VRM has reached 0.5 times and $\left(1-e^{-1}\right)$ *times its equilibrium normalized magnetization* $\mathbf{n}_{eq}$ *are indicated, the latter of which corresponds to time being equal to the relaxation time of the respective grains.*

DR4 Derivation of the effective time t_{eff} for continuous heating

Dodson (1976) and Dodson and McClelland-Brown (1980), derived an expression that relates the blocking temperature of a slowly cooling rock to the unblocking temperature during thermal demagnetization at constant temperature (as an approximation to stepwise demagnetization). Independently, York (1978a,b) derived an expression with a different approach for the same scenario that yielded equivalent results.

Here we derive an expression for the demagnetization temperature in the converse problem of continuous heating rather than continuous cooling, largely following the ideas of York (1978a,b). As continuous heating experiments is most conveniently done at a constant heating rate, the temperature at any time t is given by

$$T(t) = T_0 + rt\,, \tag{DR12}$$

where T_0 is room temperature and r is the heating rate (1°C/s, for example). Using Néel (1949) theory for single-domain (SD) magnetic particles, the relaxation time τ of an SD grain is given by

$$\frac{1}{\tau} = \frac{2}{\tau_0} \exp\left\{-\frac{\mu_0 V M_s H_K}{kT}\right\}\,, \tag{DR13}$$

where τ_0 is the atomic attempt time, μ_0 is the vacuum permeability, V is the grain volume, M_s is the spontaneous magnetization, H_K is the microscopic coercivity, and k is the Boltzmann constant. If the net number of particles magnetized in field direction (i.e., number of particles magnetized in field direction minus number of particles magnetized against field direction) is n, then the change with time t of this number is given by the differential equation

$$\frac{dn}{dt} = -\frac{n_{eq} - n}{\tau}\,, \tag{DR14}$$

where n_{eq} is the equilibrium state, which equals zero for a demagnetization experiment in zero field. The remaining magnetization $n(t)$ of the initial magnetization n_0 is therefore given by the equation

$$\ln\left(\frac{n}{n_0}\right) = \frac{2}{\tau_0} \int \exp\left\{-\frac{\mu_0 V M_s H_K}{kT}\right\} dt\,. \tag{DR15}$$

Substituting t for T by means of eq. (DR12),

$$\ln\left(\frac{n}{n_0}\right) = \frac{2}{r\tau_0} \int_{T_0}^{T} \exp\left\{-\frac{\mu_0 V M_s H_K}{kT}\right\} dT\,. \tag{DR16}$$

Assuming shape anisotropy as the dominant process responsible for the remanence (eq. DR4) and using the analytical for the spontaneous magnetization for magnetite (eq. DR5), the solution of this integral is

$$\ln\left(\frac{n}{n_0}\right) = -\frac{2}{r\tau_0} e^{\varepsilon_0/kT_C} \left[\frac{\varepsilon_0}{k}\mathrm{Ei}\left(-\frac{\varepsilon_0}{kT}\right) - \frac{\varepsilon_0}{k}\mathrm{Ei}\left(-\frac{\varepsilon_0}{kT_0}\right) + Te^{-\varepsilon_0/kT_D} - T_0 e^{-\varepsilon_0/kT_0}\right]\,, \tag{DR17}$$

where $\varepsilon_0 = \mu_0 V \Delta N V M_{s0}^2$, and Ei is the exponential integral. In this equation, the two terms containing T_0 are much smaller than the respective terms involving T, and so we can neglect them, and as ε_0/kT is somewhere in the range of 25 to 60 for grains with relaxation times between laboratory and geological time-scales, we can use the first two terms of a divergent series to approximate the exponential integral

$$\mathrm{Ei}(x) \approx \frac{e^{-x}}{x} + \frac{e^{-x}}{x^2} + \ldots\,. \tag{DR18}$$

This simplifies the equation

$$\ln\left(\frac{n}{n_0}\right) = -\frac{2T}{r\tau_0} \cdot \frac{kT}{\varepsilon_0} \exp\left\{-\frac{\varepsilon_0}{k}\left(\frac{1}{T} - \frac{1}{T_C}\right)\right\}\,. \tag{DR19}$$

In order to compare the heating rate in a continuous thermal demagnetization experiment to the timescale in a stepwise thermal demagnetization experiment, the same calculation has to be repeated for a for a constant temperature T_D held over a time interval t_D. As the integrand in eq. (DR15) is independent of time in this case,

$$\ln\left(\frac{n}{n_0}\right) = -\frac{2t_D}{\tau_0}\exp\left\{-\frac{\varepsilon_0}{k}\left(\frac{1}{T_D}-\frac{1}{T_C}\right)\right\}. \tag{DR20}$$

The two equations are equivalent if we replace the time t by an effective time

$$t_{eff} = \frac{\tau_0}{2}\exp\left\{W\left(\frac{2T}{r\tau_0}\left(1-\frac{T}{T_C}\right)\right)\right\}, \tag{DR21}$$

where W is the Lambert W function, which is defined to be the solution of $x = W(x)\,e^{W(x)}$.

DR5 Directional analysis

Most samples of the Sólheimajökull (Fig. DR5a–DR5f) and the Kotarjökull (Fig. DR5g–DR5l) showed two identifiable magnetic components. The number of samples with two components are given in Table DR12 (5 to 8 cores were sampled per boulder). Some only showed one component and were excluded from further analysis. While some samples gave clear inflection points between the two components (Fig. DR5a, DR5c, DR5d, DR5h and DR5i), others showed a curvature between them (Fig. DR5b, DR5e, DR5f, DR5g, DR5j, DR5k and DR5l). Using the algorithm described in section DR3, demagnetization temperatures could be obtained from both of them. Fig. DR5a and DR5b show two samples from the same boulder, one of them having a clear inflection point, the other displaying curvature. The algorithm (section DR3) yields similar demagnetization temperatures for both samples, with 108°C and 93°C, respectively.

Equal area projections of the VRMs and ChRMs on a per-boulder basis (Fig. DR6a–DR6f) show the directions of the individually oriented samples of the same boulder and Fisher (1953) statistics is used to calculate the mean directions and their dispersion. Boulders showed different levels of clustering of the ChRM and the VRM and those with insufficient clustering were rejected. Moreover, boulders such as the ones shown in Fig. DR6d and DR6f were excluded as the VRM did not tend towards north, as compared to the ChRM. Fig. DR7a and DR7b show the directions of the VRMs of all samples from all boulders at the two sites on equal area projections. Both figures show a significant dispersion in VRM directions, but with a statistically significant northward direction of the VRM at the 95% confidence level.

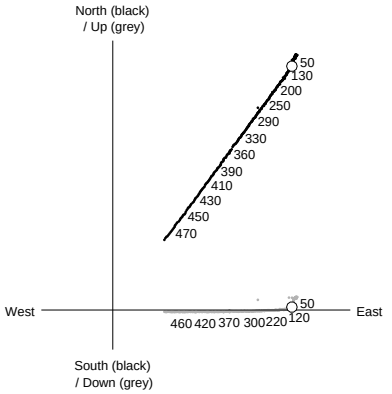

(a) Sample S14D (accepted) showing a clear blocking temperature. $T_D = 108$°C.

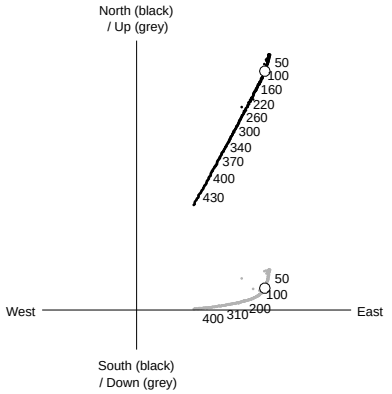

(b) Sample S14E (accepted) from the same boulder showing a strong curvature. $T_D = 93$°C.

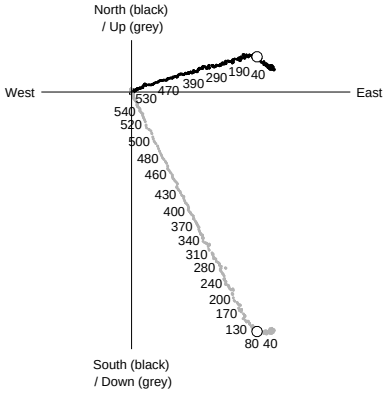

(c) Sample S15D (accepted) showing a clear blocking temperature. $T_D = 80$°C.

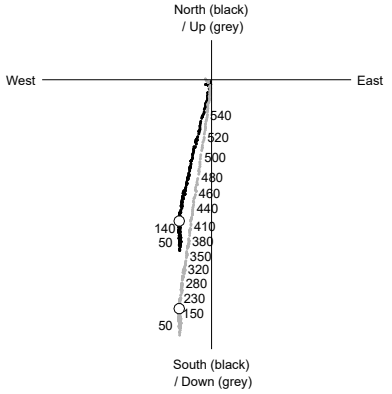

(d) Sample S19A (accepted) where VRM and ChRM are in almost the same directions. $T_D = 149$°C.

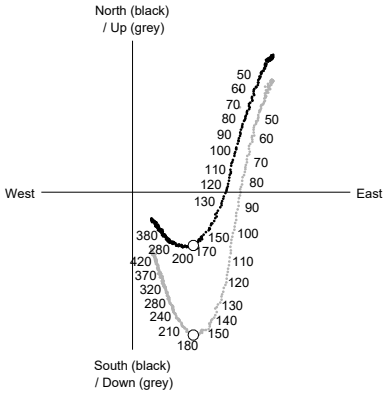

(e) Sample S21F (accepted) with a very strong curvature. $T_D = 161$°C.

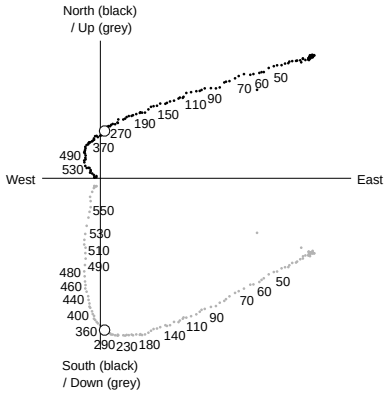

(f) Sample S01D (rejected because of disperse "VRM") showing a strong curvature. $T_D = 266$°C.

Figure DR5: Zijderveld (1967) diagrams of selected samples. Numbers along plots indicate temperatures in degrees Celsius, white circles indicate determined demagnetization temperatures T_D of the VRMs.

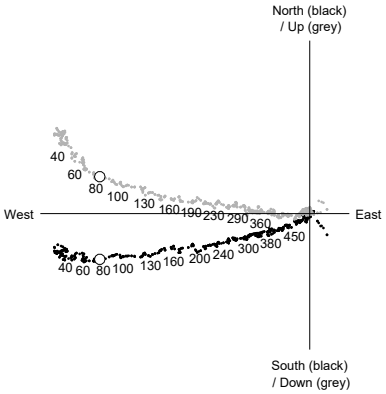

(g) Sample K06A (accepted) showing a very strong curvature. $T_D = 70°\text{C}$.

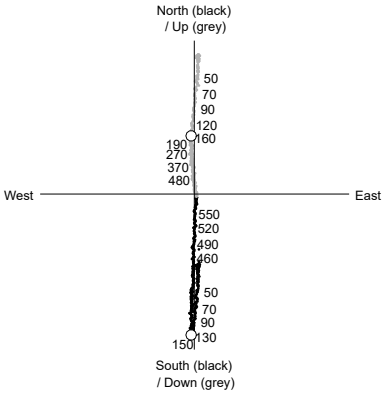

(h) Sample K09A (accepted) that rotated almost 180°, with a very clear unblocking temperature. $T_D = 139°\text{C}$.

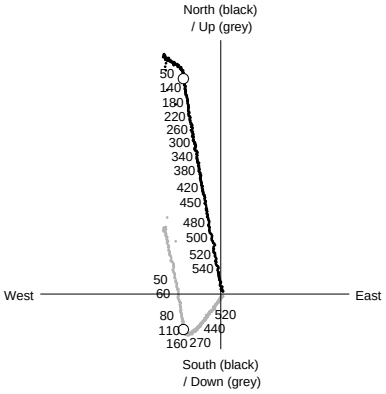

(i) Sample K11B (accepted) showing a clear blocking temperature. $T_D = 105°\text{C}$.

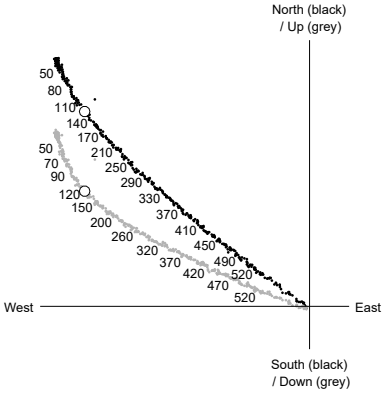

(j) Sample K13F (accepted) showing a strong curvature. $T_D = 110°\text{C}$.

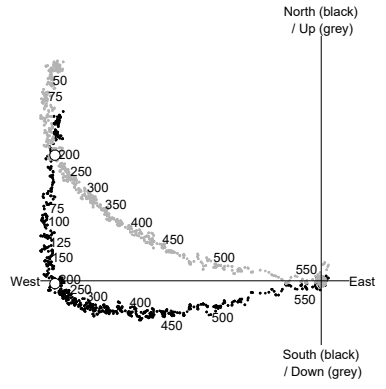

(k) Sample K17F (accepted) showing significant noise. $T_D = 187°\text{C}$.

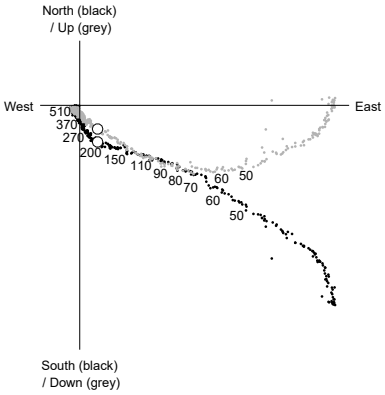

(l) Sample K08F (rejected because of $M_s(T)$) showing a complex curvature that is most likely an artefact due to the mineralogy of the sample. $T_D = 185°\text{C}$.

Figure DR5: (continued).

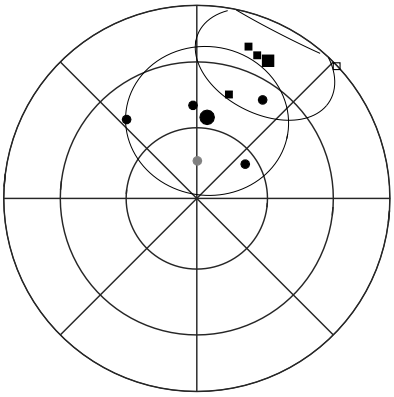

(a) Boulder S08 (accepted).

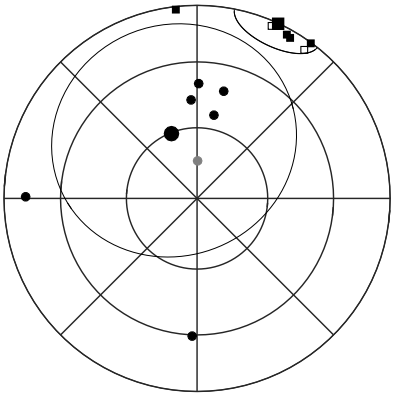

(b) Boulder S14 (accepted): weak but sufficient clustering of VRM.

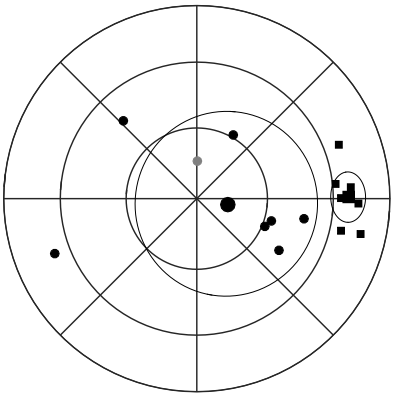

(c) Boulder S20 (accepted): weak but sufficient clustering of VRM.

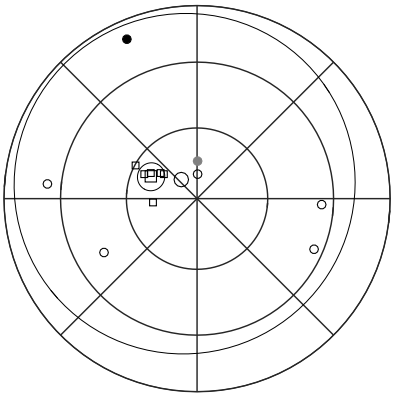

(d) Boulder K04 (rejected): very disperse VRM that does not tend towards the northward.

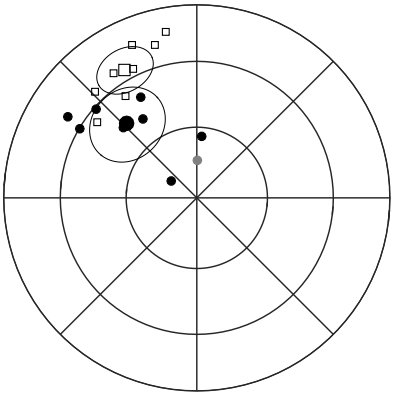

(e) Boulder K11 (accepted).

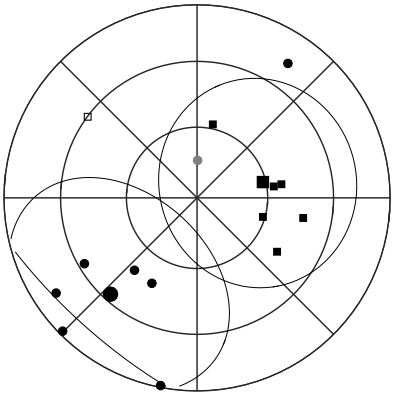

(f) Boulder K20 (rejected): weak clustering, and VRM not tending northward.

Figure DR6: Equal area projections, indicating the directions of the VRMs (squares) and the ChRM (circles), together with their mean directions calculated from Fisher (1953) statistics (bold symbols). Each plot shows all samples (dots) of one boulder. Open symbols are in the upper (southern) hemisphere, closed symbols in the lower (northern) hemisphere. Grey circle indicates present-day field direction for the location.

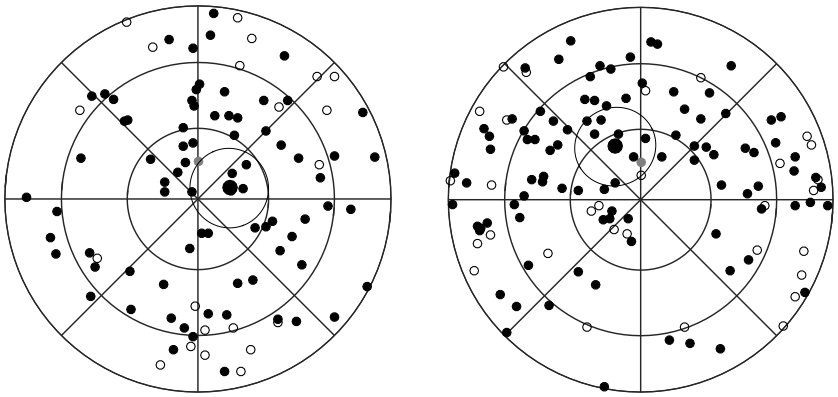

(a) All samples of all (accepted and rejected) boulders from the Sólheimajökull.

(b) All samples of all (accepted and rejected) boulders from the Kotarjökull.

Figure DR7: Equal area projections, indicating the directions of the VRMs of all samples of all boulders (circles), together with their mean directions calculated from Fisher (1953) statistics (bold symbols). Open symbols are in the upper (southern) hemisphere, closed symbols in the lower (northern) hemisphere. Grey circle indicates present-day field direction for the location.

DR6 Rock magnetic results

Standard rock magnetic and viscosity experiments were done on one sample of each boulder on a Princeton Vibrating Sample Magnetometer (VSM). For the floods at the Sólheimajökull and the Kotarjökull, the thermomagnetic curves showed a shape (Fig. DR8a–DR8f) and Curie temperature indicating predominantly magnetite, with a median T_C of 567°C and 593.5°C, respectively (only accepted samples according to quality criteria, Fig. DR8a–DR8f). Given that the thermocouple in the Princeton VSM is a few millimeters below the sample, the sample experiences a thermal lag during heating and cooling that introduces a temperature uncertainty we estimate at ~ 10°C. Most curves were reversible (Fig. DR8b, DR8d), were some showed slight thermochemical alterations on heating (Fig. DR8a). A few samples showed curves like the one shown in Fig. DR8c with a steep decay at low temperatures and slowly decaying to zero at high temperatures, indicating a mixture of magnetic minerals and were excluded from further analysis.

Hysteresis parameters plotted on a Day plot (Day et al., 1977) show that almost all samples contain a mixture of SD and MD grains and/or PSD grains. To resolve the ambiguity between PSD grains and SD+MD mixtures FORC diagrams (Roberts et al., 2000) were measured for most of the boulders (Fig. DR10a–DR10d) and fitted with a smoothing factor of $SF = 3$ using the software by Zhao et al. (2015).

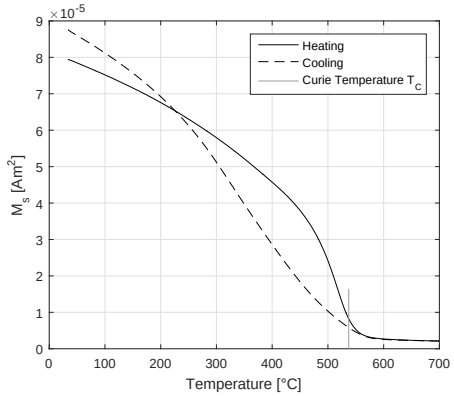

(a) Boulder S8 (accepted) showing a clear Curie temperature but some thermal alterations on heating.

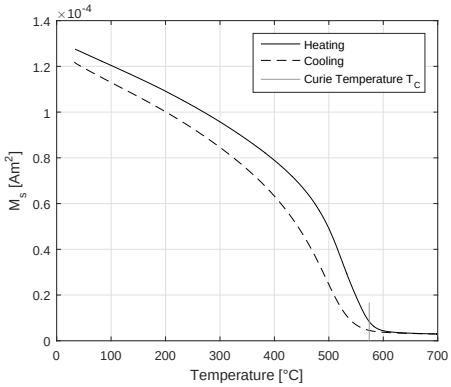

(b) Boulder S19 (accepted) showing a very clear Curie temperature and a shape typical for magnetite.

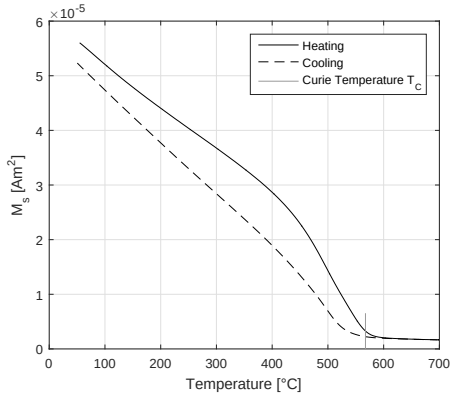

(c) Boulder S24 (accepted) showing a relatively clear Curie temperature.

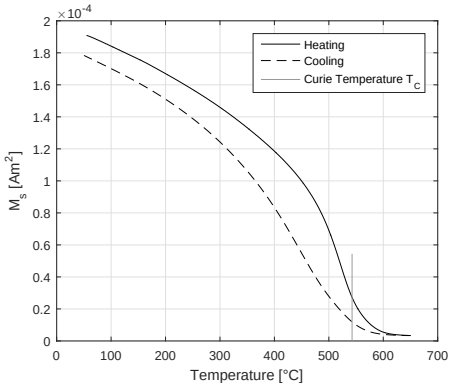

(d) Boulder K4 (rejected because of directional criteria) showing a very clear Curie temperature and a shape typical for magnetite.

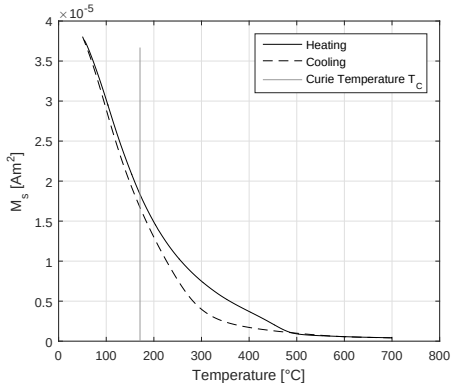

(e) Boulder K14 (rejected) showing no clear Curie temperature, but a steep decay at low temperatures, slowly approaching zero at high temperatures.

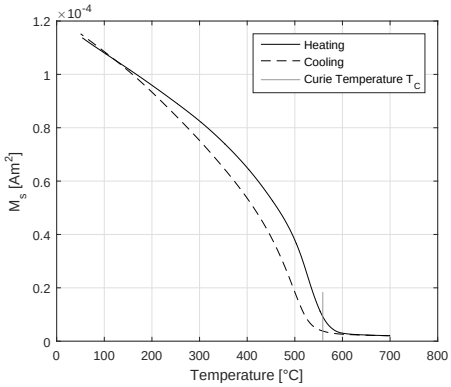

(f) Boulder K17 (accepted) showing a very clear Curie temperature and a shape typical for magnetite.

Figure DR8: Spontaneous magnetization as a function of temperature $M_s(T)$ as determined in a 1 T field, together with their Curie temperatures determined by the method of maximum second derivative (Ade-Hall et al., 1965). Cooling curves appear slightly offset towards lower temperature because of thermal lag.

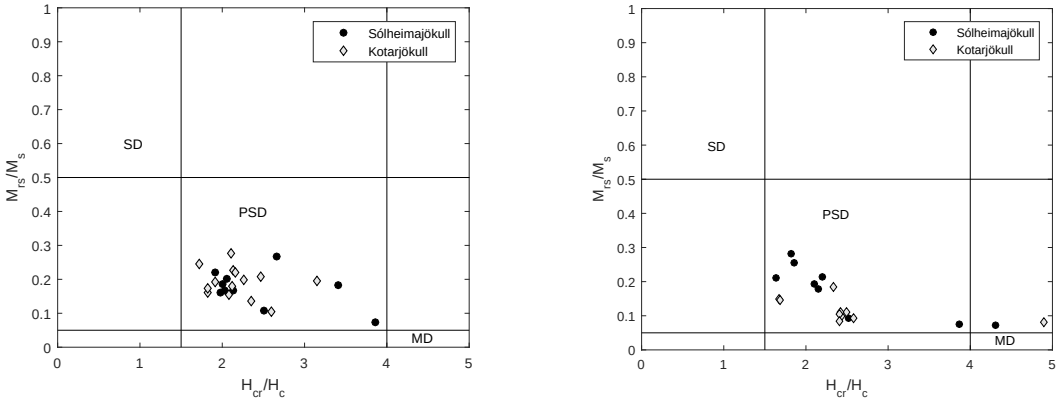

(a) All accepted samples.

(b) All rejected samples.

Figure DR9: Day plots.

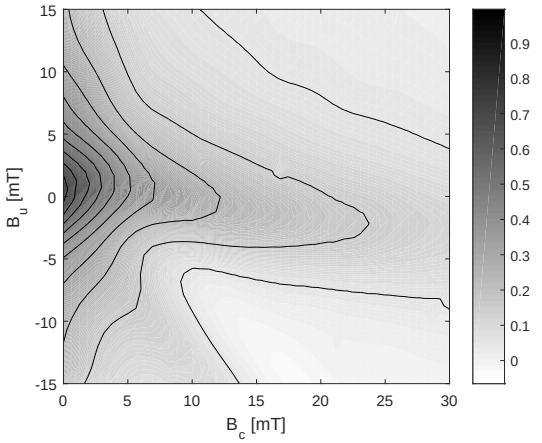

(a) Boulder S17 (accepted) showing mostly superparamagnetic grains.

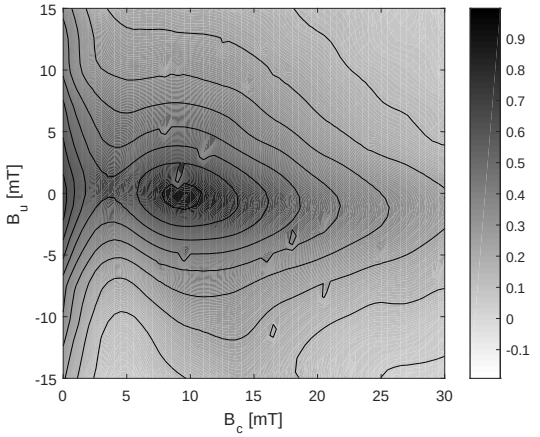

(b) Boulder S23 (accepted) showing a mixture of single-domain (SD) and superparamagnetic (SP) grains.

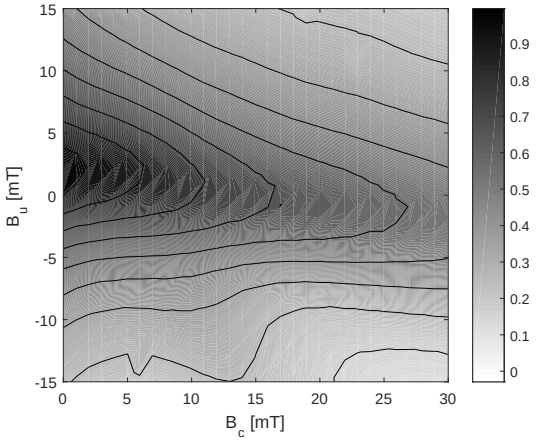

(c) Boulder K11 (accepted) showing a dominant multi-domain (MD) behaviour.

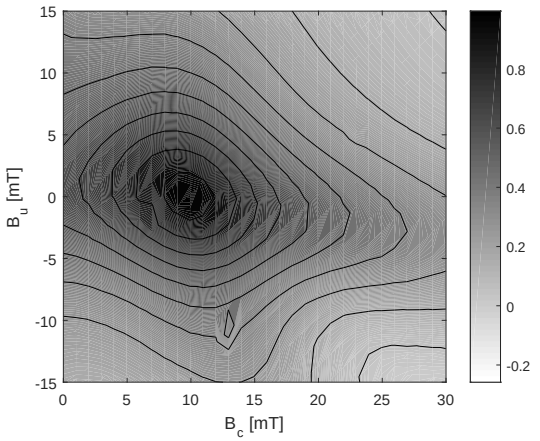

(d) Boulder K18 (rejected because of directional criteria) showing a dominant interacting single-domain (SD) behaviour.

Figure DR10: First-order reversal-curves (Roberts et al., 2000, SF=3, measurement time 100 ms) used to assess domain states. The FORC distributions are normalized by their peak values.

DR7 Viscosity experiments

The effective attempt time $\tau_{0,eff}$ was determined from Zijderveld (1967) plots constructed from the viscosity experiments (Fig. DR11). Using these values, nomograms can be plotted for each of the boulders with the best fit $\tau_{0,eff}$. Fig. DR12 shows these together with the acquisition and demagnetization times and temperatures from the viscosity experiments. In most cases longer acquisition times lead to higher demagnetization temperatures as expected from eq. (DR1), but some samples (Fig. DR12b) show a few "crossing over" data points. This would imply that a longer acquisition time leads to a lower demagnetization temperature, which is very unlikely. This effect is probably due to two factors: (1) noise, in particular regarding the temperature accuracy between different VRM acquisition experiments, as the temperature control is much lower for the three-component high-temperature VSM ($\gg$ 1°C) compared to the MPMS ($<$0.5°C), and (2) to thermochemical alterations occurring during each of the successive VRM acquisition experiments. In particular for short acquisition times, where demagnetization temperatures are close to acquisition temperatures, slight variations in temperature and heating rate can cause comparably large deviations. Nevertheless, all data points were included, leaving it up to the statistics of a large number of viscosity measurements to reduce errors.

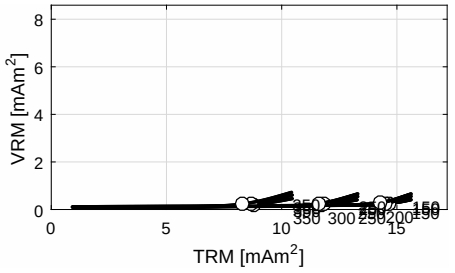

(a) Boulder S18 (accepted).

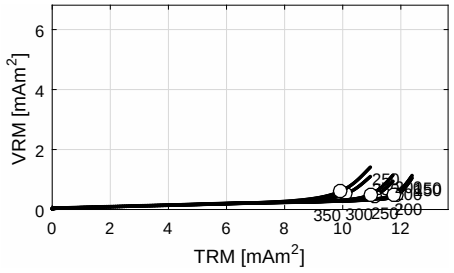

(b) Boulder K01 (accepted).

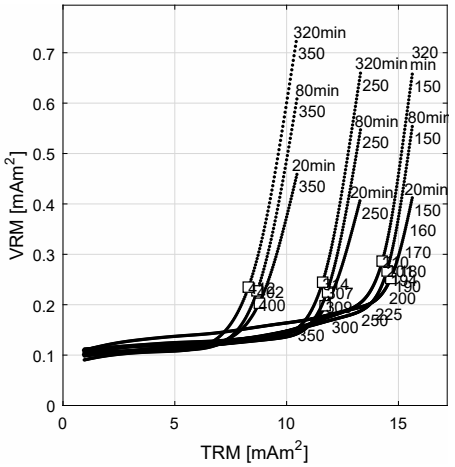

(c) Boulder S18 (accepted).

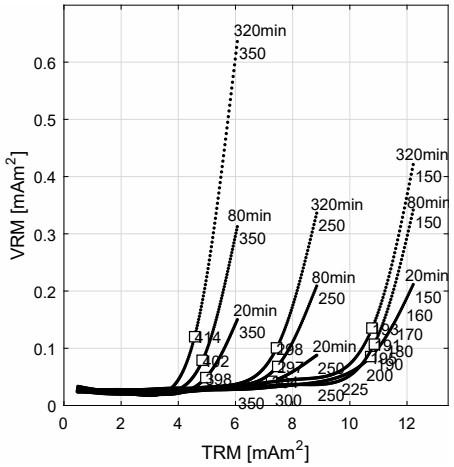

(d) Boulder S20 (accepted).

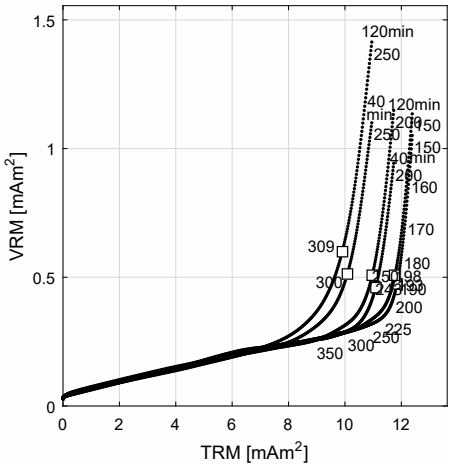

(e) Boulder K01 (accepted).

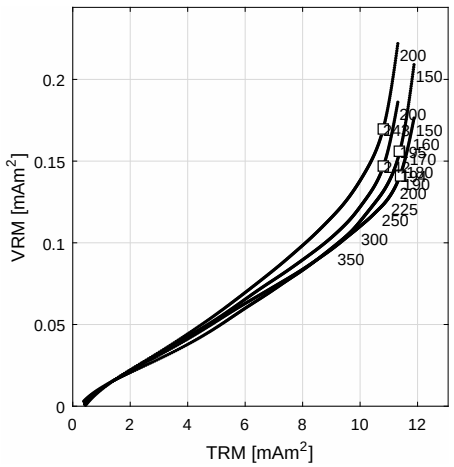

(f) Boulder K08 (rejected because of directional criteria).

Figure DR11: Zijderveld (1967) plots created from CTD of various laboratory VRMs acquired at different temperatures T_i (temperature given in °C at the top of each of the plots) and time t_i (times given in minutes at the top of each plot). Plots are created by plotting the VRM on the vertical axis, and a full laboratory TRM on the horizontal axis. Fig. DR11a and DR11b are drawn to scale; all other figures a drawn with a magnified y-axis. Demagnetization temperatures (circles) correspond to points where the direction vector is halfway between the initial (low temperature) direction and the final (high temperature) direction, but visually appear to be at lower temperatures due to the different axes.

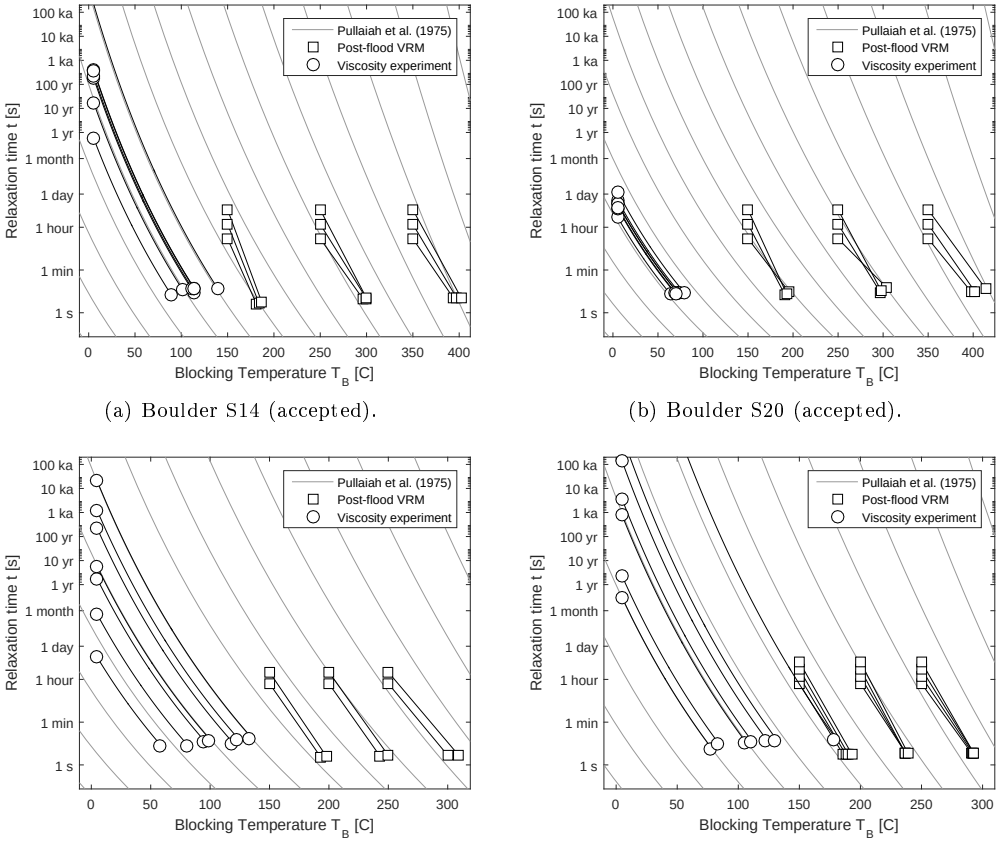

(a) Boulder S14 (accepted).

(b) Boulder S20 (accepted).

(c) Boulder K01 (accepted).

(d) Boulder K06 (accepted).

Figure DR12: Nomograms showing the acquisition/demagnetization times/temperatures of the viscosity experiments (squares, all data are from the same sample for each boulder). Pullaiah et al. (1975) nomogram contour lines are plotted using the effective attempt time $\tau_{0,eff}$ that best fits the experimental data. Circles indicate demagnetization time and temperature of the post-flood natural VRMs of all samples of the boulder (4–7 samples) and are extrapolated to the ambient average temperature at the field location using eq. (DR1) with $\tau_{0,eff}$.

DR8 Summary of boulders

Tables DR12 and DR12 summarize the rock magnetic properties determined for one sample per boulder, together with the directional analysis and determined $\tau_{0,eff}$ and age estimates.

Table DR12: Summary of directional analysis, Curie temperatures and ages obtained for all analysed boulders of the Sólheimajökull (S) and Kotarjökull (K) floods. N: number of samples with identifiable VRM per boulder; Zijderveld: quantitative description of Zijderveld (1967) plots; Δ: difference between the angular distance of the VRM to the actual northward direction and the NRM and to the actual northward direction (negative numbers indicate the the NRM is closer to the north than the VRM); VRM and TRM α_{95}: clustering in degrees (TRM refers to the pre-flood / high-temperature magnetic component); T_C, $\tau_{0,eff}$, domain state: Curie temperature, effective attempt time and interpretation of FORC diagrams (Roberts et al., 2000) of one sample per boulder, uncertainties refer to one standard deviation of a bootstrap of $\tau_{0,eff}$ viscosity experiments; age: median age estimate for all samples from the boulder, uncertainties are one standard deviation of a bootstrap of all samples of the boulders. Numbers in brackets indicate values that did not pass the quality criteria such that these boulders were excluded from analysis. Bottom two lines give median values of all, and only of samples that passed the quality criteria, respectively (not using bootstrap method, section DR9), i.e. median values of each column of the table. See text for a discussion of error limits.

Boulder	N	Zijderveld	Δ[°]	TRM α_{95}	VRM α_{95}	T_C [°C]	$\tau_{0,eff}$ [s]	Domain state	Age [yr]	Reject
S1	5	curved	90	42	*(86)*	521	$4 \times 10^{-9\pm0.7}$	SD	$4.8 \times 10^{41\pm21}$	X
S2	7	clear	27	*(65)*	50	569	$1 \times 10^{-6\pm0.8}$	SD+MD	$1.5 \times 10^{7\pm11}$	X
S3	4	clear	73	48	*(121)*	*(217)*	$3 \times 10^{-6\pm0.3}$	SP	$2.2 \times 10^{95\pm49}$	X
S4	6	curved	*(-9)*	*(95)*	*(86)*	*(211)*	$6 \times 10^{-5\pm0.3}$	–	$13 \times 10^{\pm0.1}$	X
S5	4	curved	*(-25)*	*(100)*	*(73)*	572	$2 \times 10^{-19\pm1.5}$	SP	$2.2 \times 10^{11\pm3}$	X
S7	4	clear	113	*(127)*	*(73)*	542	$3 \times 10^{-18\pm1.0}$	MD	$9.5 \times 10^{5\pm0.1}$	X
S8	4	curved	36	26	33	537	$2 \times 10^{-10\pm1.3}$	–	$5.9 \times 10^{11\pm3}$	–
S14	7	clear	60	14	52	583	$4 \times 10^{-12\pm1.8}$	–	$210 \times 10^{\pm0.6}$	–
S15	8	clear	19	3	23	585	$1 \times 10^{-11\pm1.2}$	SP	$0.9 \times 10^{\pm0.3}$	–
S16	7	curved	30	8	30	*(132)*	–	–	5800	X
S17	4	clear	23	10	56	554	$7 \times 10^{-18\pm1.7}$	PSD	$1400 \times 10^{\pm0.3}$	–
S18	1	clear	86	–	–	533	$9 \times 10^{-6\pm0.7}$	–	2.8×10^{-3}	–
S19	2	clear	22	9	26	574	$6 \times 10^{-6\pm0.7}$	–	38	–
S20	7	curved	46	9	39	570	$8 \times 10^{-9\pm1.1}$	SP+MD	$1.1 \times 10^{-3\pm0.01}$	–
S21	4	clear	145	12	19	506	$7 \times 10^{-7\pm1.3}$	PSD	$43000 \times 10^{\pm0.1}$	–
S22	2	curved	26	15	56	541	$1 \times 10^{-4\pm1.2}$	SD	10	–
S23	6	curved	13	12	13	568	$6 \times 10^{-8\pm0.7}$	SP+SD	$4.8 \times 10^{7\pm0.4}$	–
S24	7	clear	37	8	22	567	$3 \times 10^{-8\pm0.9}$	SP+SD	$140 \times 10^{\pm1.3}$	–
S25	3	curved	17	22	18	*(372)**	$2 \times 10^{-5\pm0.4}$	–	$240 \times 10^{\pm12}$	X
S27	6	clear	13	7	26	590	$5 \times 10^{-8\pm1.6}$	SP+SD	$34 \times 10^{\pm0.5}$	–
All S	4.5		28.5	14	39	548	5×10^{-8}		800	
Accept	4		26	11	26	567	5×10^{-8}		140	

*Boulder S25 had two distinct Curie temperatures at 371 and 513°C and showed strong thermal alterations on heating.

Table DR12: See Table DR12 caption.

Boulder	N	Zijderveld	Δ [°]	TRM α_{95}	VRM α_{95}	T_C [°C]	$\tau_{0,eff}$ [s]	Domain state	Age [yr]	Reject
K1	7	clear	7	40	30	585	$2\times10^{-11\pm0.7}$	MD	$5.5\times10^{\pm0.5}$	–
K2	4	curved	46	16	*(87)*	535	$7\times10^{-9\pm0.3}$	–	$4.7\times10^{15\pm3}$	X
K3	7	curved	15	9	15	550	$1\times10^{-13\pm1.0}$	MD	$4.3\times10^{6\pm6}$	–
K4	7	clear	*(-7)*	6	*(77)*	543	$2\times10^{-8\pm0.8}$	SD+MD	$1.9\times10^{-3\pm2}$	X
K5	1	curved	7	–	–	600	$2\times10^{-10\pm0.4}$	PSD	290	–
K6	7	curved	48	7	25	516	$3\times10^{-13\pm0.7}$	SP+SD	$3600\times10^{\pm3}$	–
K7	7	clear	15	10	12	525	$4\times10^{-4\pm0.4}$	PSD	$0.4\times10^{\pm4}$	–
K8	4	curved	39	10	37	*(261)*	–	PSD	$2.4\times10^{21\pm10}$	X
K9	5	S shape	80	15	38	585	$1\times10^{-9\pm0.2}$	MD	$920\times10^{\pm0.6}$	–
K10	1	clear	19	5	11	*(203)*	–	PSD	3.5×10^{4}	X*
K11	8	clear	67	11	16	594	$1\times10^{-14\pm1.3}$	PSD	$63\times10^{\pm0.7}$	–
K12	5	curved	4	4	18	*(227)*	–	PSD	$9.2\times10^{16\pm0.6}$	X
K13	5	clear	25	39	49	593	$7\times10^{-9\pm0.4}$	SP+SD	$96\times10^{\pm7}$	–
K14	5	curved	1	43	34	*(171)*	–	PSD	1.9×10^{9}	X*
K15	2	curved	22	–	–	596	$6\times10^{-16\pm0.8}$	SP+SD	260	–
K16	7	curved	99	31	*(360)*	520	$1\times10^{-11\pm0.5}$	SD	$0.1\times10^{\pm0.3}$	X
K17	6	curved	29	7	12	559	$3\times10^{-12\pm0.8}$	MD	$5.4\times10^{13\pm0.5}$	–
K18	2	curved	*(-25)*	*(360)*	*(360)*	543	$6\times10^{-11\pm0.4}$	SD	15000	X
K19	7	clear	57	35	31	597	$6\times10^{-16\pm1.3}$	PSD	$4400\times10^{\pm2}$	–
K20	7	curved	*(-40)*	44	46	597	$3\times10^{-16\pm0.9}$	MD	$0.1\times10^{\pm0.6}$	X
K21	6	clear	8	7	9	607	$9\times10^{-16\pm1.1}$	MD	$51\times10^{\pm0.2}$	–
K22	6	clear	53	31	43	601	$9\times10^{-18\pm1.7}$	MD	$18\times10^{\pm0.04}$	–
K23	7	curved	39	10	21	*(179)*	–	PSD	2.1	X*
K24	4	clear	62	9	41	594	$6\times10^{-18\pm0.7}$	PSD	$2.2\times10^{15\pm4}$	–
All K	6		23.5	10.5	32.5	554.5	3×10^{-12}		610	
Accept	6		27	10.5	27.5	593.5	2×10^{-13}		280	

*Almost no unblocking in the region of interest between 200° and 350°.

DR9 Two-step bootstrap method for statistical error analysis

From all individual age estimates determined for each sample, a single age for the flood needs to be calculated. The approach by Muxworthy et al. (2015) to calculate the median of all age estimates achieves this, but neglects the underlying statistical distribution of the age estimates. A full statistical treatment of the variation from sample to sample is, however, difficult because the variation of the age estimate is unlikely to follow a normal distribution (as the age in eq. (DR1) depends exponentially on T_A and T_D, but linearly on t_D, and in a non-trivial way on the parameters used to calculate τ_0). The distribution is further complicated by the fact that ages from samples of the same boulder are likely correlated and tend to yield more similar ages than samples of different boulders. If different numbers of samples are taken from each boulder, this leads to different statistical weights. Hence, the median is unlikely to best represent the flood age. Additionally, calculations of statistical error limits such as percentiles are inaccurate without knowledge of the underlying distribution. Muxworthy et al. (2015), investigated how uncertainties in the temperature in the field T_A, the attempt time τ_0, the demagnetization temperature T_D, the demagnetization timescale t_D, and the Curie temperature propagate into the age estimate t_A, but an analysis of the observed variance of age estimates requires a more advanced statistical method.

As the underlying distribution is unknown, we developed a two-step bootstrap method, where series of random re-samples are taken from the set of all measurements to obtain an estimate of the underlying distribution and from that a maximum-likelihood age estimate and error limits (Efron and Tibshirani, 1994).

As the first step, for each boulder, the individual samples are randomly re-sampled (with replacement) one thousand times and the median boulder ages for each re-sample are calculated. This approximates the error distribution of each individual boulder. Second, for each of these median boulder ages, one thousand re-samples (with replacement) are taken and the median of the median boulder ages is calculated, representing the site/flood median age. This makes a total of one million re-samples taken into account both the sample-to-sample variation of each individual boulder, and the boulder-to-boulder variation of the site. The age estimate of the flood is then the median of this distribution and the error limits corresponding to one standard deviation are the 68% quantiles of the distribution. The distributions for the two floods are shown in Fig. DR13.

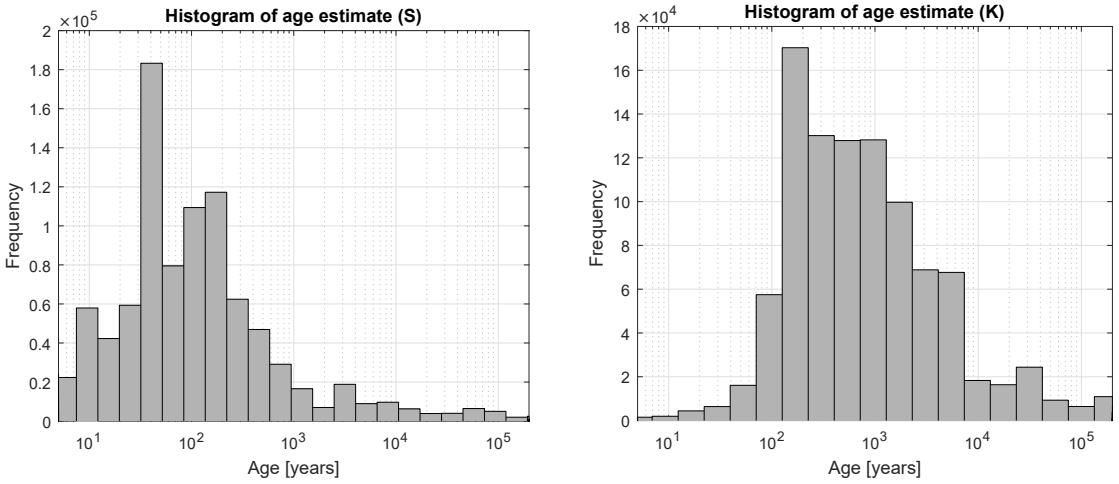

(a) Sólheimajökull. (b) Kótarjökull.

Figure DR13: Histograms showing the frequencies of median age estimates in the two-step bootstrap for the Sólheimajökull and the Kotarjökull floods (out of one million re-samples).

References

J. M. Ade-Hall, R. L. Wilson, and P. J. Smith. The petrology, Curie points and natural magnetizations of basic lavas. *Geophysical Journal International*, 9(4):323–336, 1965. doi: 10.1111/j.1365-246X.1965.tb03890.x.

R. Day, M. Fuller, and V. A. Schmidt. Hysteresis properties of titanomagnetites: Grain-size and compositional dependence. *Physics of the Earth and Planetary Interiors*, 13(4):260–267, 1977. doi: 10.1016/0031-9201(77)90108-X.

M. Dodson. Kinetic processes and thermal history of slowly cooling solids. *Nature*, 259:551–553, 1976. doi: 10.1038/259551a0.

M. H. Dodson and E. McClelland-Brown. Magnetic blocking temperatures of single-domain grains during slow cooling. *Journal of Geophysical Research*, 85:2625–2637, 1980. doi: 10.1029/JB085iB05p02625.

D. J. Dunlop and Ö. Özdemir. *Rock Magnetism: Fundamentals and Frontiers*. Cambridge University Press, Cambridge, UK, 1997. ISBN 0521325145.

B. Efron and R. Tibshirani. *An introduction to the bootstrap*. Chapman & Hall, 1994.

R. Enkin and D. Dunlop. The demagnetization temperature necessary to remove viscous remanent magnetization. *Geophysical Research Letters*, 15(5):514–517, 1988. doi: 10.1029/GL015i005p00514.

R. Fisher. Dispersion on a sphere. *Proceedings of the Royal Society of London A: Mathematical, Physical and Engineering Sciences*, 217(1130):295–305, 1953. doi: 10.1098/rspa.1953.0064.

D. Kent. Thermoviscous remagnetization in some Appalachian limestones. *Geophysical Research Letters*, 12(12):3–6, 1985. doi: 10.1029/GL012i012p00805.

D. Kent and J. Miller. Redbeds and thermoviscous magnetization theory. *Geophysical Research Letters*, 14(4):327–330, 1987. doi: 10.1029/GL014i004p00327.

M. Middleton and P. Schmidt. Paleothermometry of the Sydney basin. *Journal of Geophysical Research*, 87(2):5351–5359, 1982. doi: 10.1029/JB087iB07p05351.

A. R. Muxworthy, J. Williams, and D. Heslop. Testing the use of viscous remanent magnetisation to date flood events. *Frontiers in Earth Science*, 3:1–9, 2015. doi: 10.3389/feart.2015.00001.

L. Néel. Théorie du traînage magnétique des ferromagnétiques en grains fins avec applications aux terres cuites. *Annales de Géophysique*, 1949. doi: 10.1016/S0009-2509(00)00427-9.

G. Pullaiah, E. Irving, K. Buchan, and D. Dunlop. Magnetization changes caused by burial and uplift. *Earth and Planetary Science Letters*, 28:133–143, 1975. doi: 10.1016/0012-821X(75)90221-6.

A. Roberts, C. R. Pike, and K. L. Verosub. First-order reversal curve diagrams: A new tool for characterizing the magnetic properties of natural samples. *Journal of Geophysical Research*, 105: 28,461–28,475, 2000.

T. Sato, N. Nakamura, K. Goto, Y. Kumagai, H. Nagahama, and K. Minoura. Paleomagnetism reveals the emplacement age of tsunamigenic coral boulders on Ishigaki Island, Japan. *Geology*, 42 (7):603–606, 2014. doi: 10.1130/G35366.1.

R. T. Smith and K. L. Verosub. Thermoviscous remanent magnetism of Columbia River basalt blocks in the cascade landslide. *Geophysical Research Letters*, 21(24):2661–2664, dec 1994. doi: 10.1029/94GL02669.

D. Walton. Time-temperature relations in the magnetization of assemblies of single domain grains. *Nature*, 286(5770):245–247, 1980. doi: 10.1038/286245a0.

D. York. Magnetic blocking temperature. *Earth and Planetary Science Letters*, 39:94–97, 1978a. doi: 10.1016/0012-821X(78)90145-0.

D. York. A formula describing both magnetic and isotopic blocking temperatures. *Earth and Planetary Science Letters*, 39:89–93, 1978b. doi: 10.1016/0012-821X(78)90144-9.

X. Zhao, D. Heslop, and A. P. Roberts. A protocol for variable-resolution first-order reversal curve measurements. *Geochemistry, Geophysics, Geosystems*, 16(5):1364–1377, 2015. doi: 10.1002/2014GC005680.

J. Zijderveld. AC demagnetization of rocks: analysis of results. In D. Collinson, K. Creer, and S. Runcorn, editors, *Methods in paleomagnetism*, pages 254–286. 1967.